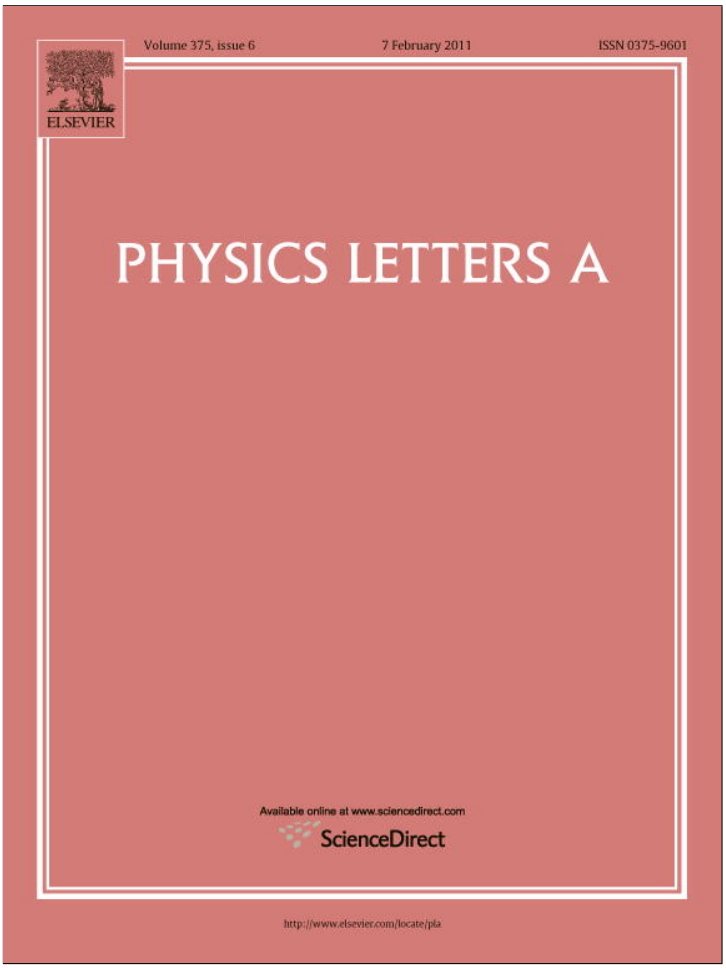

Physics Letters A 375 (2011) 1014–1018

Contents lists available at ScienceDirect

Physics Letters A

www.elsevier.com/locate/pla

Backward electronic Tamm states in graphene-based heterostructures

Hai-tao Jiang [a,b,*], Zi-li Wang [a,b], Zhi-guo Wang [a,b], Hong Chen [a,b]

[a] Pohl Institute of Solid State Physics, Tongji University, Shanghai 20092, People's Republic of China
[b] Key Laboratory of Special Artificial Microstructure Materials and Technology, Tongji University, Shanghai 200092, People's Republic of China

ARTICLE INFO

Article history:
Received 9 December 2010
Received in revised form 29 December 2010
Accepted 29 December 2010
Available online 31 December 2010
Communicated by V.M. Agranovich

Keywords:
Backward waves
Surface waves
Graphene

ABSTRACT

We study the electronic surface waves (the so-called Tamm states) localized at the interface between a graphene-based superlattice and a homogeneous graphene by applying suitable electrodes on a graphene sheet. The magnitude as well as the sign of the slope of the Tamm dispersive curve can be flexibly tuned just by varying the external voltage. Particularly, in addition to the conventional forward Tamm states, backward Tamm states in which the wave vector of the electronic surface wave is antiparallel with the group velocity can be realized.

1. Introduction

Recently, a monolayer of carbon atoms arranged in a honeycomb pattern called graphene has attracted people's great interest due to its unique electronic properties [1]. The hexagonal symmetry of graphene, in which the unit cell contains two equivalent carbon atoms, can make the valence and conduction bands cross at a point. This special point is also called a Dirac point around which the electrons behave like massless Dirac particles obeying a linear energy dispersion relation [1–4]. The Dirac electrons possess many unusual properties such as ballistic conduction [1], Klein tunnelling [3,4], peculiar quantum Hall effect [5], gate-variable optical transitions [6], and so on. Particularly, in the valence band below the Dirac point, the direction of the wave vector of an electron wave is opposite to that of the group velocity. This electronic property is very similar to that of a photon in a left-handed metamaterial in which the relative direction of the wave vector and the group velocity of an electromagnetic (EM) wave is antiparallel [7]. In the conduction band above the Dirac point, the wave vector and the group velocity have the same direction. By applying a gate voltage to a graphene sheet, the Fermi level in the previous Dirac point can be lowered into the valence band or raised into the conduction band, leading to a p-type or n-type conductor. In graphene p–n junctions, the electron flow can be negatively refracted [8], similar to the negative refraction appearing at the interfaces due to the negative group velocity of light in one of the interfacing media (see Ref. [9] and references therein). Moreover, by varying the gate voltage in an n–p–n junction of a graphene transistor, the device can be used as an electron beam splitter or a collimator [10] or a spin lens if ferromagnetic graphene is included [11].

Furthermore, graphene-based superlattices with periodic potential patterns can be realized by various ways such as applying electrostatic potentials [12–16] or magnetic barriers [17,18] or introducing periodic corrugations on a graphene sheet [19]. In practice, superlattice patterns have been achieved by the electron-beam induced deposition on a graphene [20]. Periodically rippled graphene has also been epitaxially grown on some metal surfaces [21,22]. With the progress of growing large-scale graphene [23], graphene sheets with periodically patterned gate electrodes may be another way to obtain graphene-based superlattices. Similar to other superlattices [24], graphene-based superlattices give us more freedom to control the electronic properties. For example, strong anisotropy for the group velocities of electrons [13], tunable quantum-Hall effect associated with new Dirac electrons [25,26], and adjustable band gaps [27] can occur in graphene-based superlattices. Collimations of electron beam [28,29] and non-Bragg electronic gap insensitive to the lattice constant [30] are also found to exist in graphene-based superlattices.

The concepts in electronic field and photonic field can inspire each other. As mentioned before, the negative refraction of electrons is induced by the concept of negative refraction of EM waves in metamaterials. On the other hand, inspired by the graphene, a two-dimensional photonic crystal (PhC) with honeycomb pattern has been proposed [31]. The 'photonic graphene' has many photonic properties similar to the properties of Dirac electrons such as nonreciprocal EM states [31,32], pseudodiffusive transport of

* Corresponding author at: Pohl Institute of Solid State Physics, Tongji University, Shanghai 20092, People's Republic of China.
E-mail address: jiang-haitao@tongji.edu.cn (H.-t. Jiang).

0375-9601/$ – see front matter
doi:10.1016/j.physleta.2010.12.073

light [33], etc. Another example is Tamm states, localized electronic states formed at the edge of a truncated periodic atomic potential [34]. The terminated solid introduces additional perturbation to the periodic potential and causes an asymmetric potential and thereby a localized state at the surface. Tamm states were firstly observed by Ohno et al. in a semiconductor superlattice [35]. On the other hand, the periodic impedance in a PhC can be considered as periodic optical potential. In analogy with the electronic Tamm states, localized EM states at the surface of a truncated PhC, so-called optical Tamm states (OTSs), have been proposed [36–39]. Recently, Namdar et al. studied the OTSs at the interface of a truncated one-dimensional PhC and a homogeneous left-handed metamaterial [40]. They found the metamaterial can tune the dispersive properties of the OTSs flexibly and even support backward OTSs in which the direction of the wave vector and the group velocity of the surface EM wave is antiparallel. From electronic Tamm states, people discover OTSs and even backward OTSs. Now can we return back to the electronic field and find backward electronic Tamm states?

In this Letter, we use a homogeneous graphene applied by an electrode whose potential exceeds the energy of the incident electrons as a left-handed electronic medium in which the direction of the wave vector of the electron wave is opposite to that of group velocity. Then we study the Tamm states localized at the interface between the left-handed graphene and a graphene-based superlattice. The left-handed graphene tuned by external voltage allows for a flexible control of the dispersive properties of Tamm state and especially can support backward Tamm states in which the wave vector of the electronic surface wave reverses with the group velocity. The Letter is organized as follows. In Section 2, we deduce the dispersion equation for Tamm states in the graphene-based heterostructures. Then, in Section 3 we numerically calculate the dispersion diagram and the probability amplitude patterns. Finally, we conclude in Section 4.

2. Dispersion equation for Tamm states

If we apply an electrostatic potential $V(x)$ varying with the coordinate x on a graphene sheet, the Hamiltonian of the Dirac electron can be written as

$$\hat{H} = \upsilon_F \boldsymbol{\sigma} \bullet \mathbf{p} + V(x)\hat{I}, \tag{1}$$

where $\boldsymbol{\sigma} = (\sigma_x, \sigma_y)$ with σ_x, σ_y being Pauli matrices of the pseudospin, $\mathbf{p} = (p_x, p_y) = (-i\hbar\frac{\partial}{\partial x}, -i\hbar\frac{\partial}{\partial y})$ is the momentum operator with the x and y components, $\upsilon_F \approx 10^6$ m/s is the Fermi velocity, and $\hat{I}$ is a 2×2 unit matrix. $\hat{H}$ acts on a state denoted by a pseudospinor $\boldsymbol{\psi} = (\tilde{\psi}_A, \tilde{\psi}_B)^T$, where $\tilde{\psi}_{A,B}(x,y) = \psi_{A,B}(x)e^{i\beta y}$ are the wave functions for two triangular sublattices in graphene, with β being the wave vector along the y coordinate. From Eq. (1), one can obtain

$$\frac{d\psi_A}{dx} - \beta\psi_A = ik\psi_B, \tag{2}$$

$$\frac{d\psi_B}{dx} + \beta\psi_B = ik\psi_A, \tag{3}$$

where $k = [E - V(x)]/\hbar\upsilon_F$ is the wave vector inside graphene, E is the energy of an incident electron. If $E < V(x)$, the direction of k inside the barrier will be opposite to that of group velocity and the graphene becomes a left-handed electronic medium.

Now we deduce the dispersion equation for Tamm states. The graphene-based heterostructure is schematically shown in Fig. 1. The heterostructure is composed of a homogeneous graphene S applied by a potential of V_s and an (AB) graphene superlattice in which A and B regions are applied by potentials of V_1 and V_2, respectively. The thicknesses of A and B regions are denoted by d_1 and d_2, respectively.

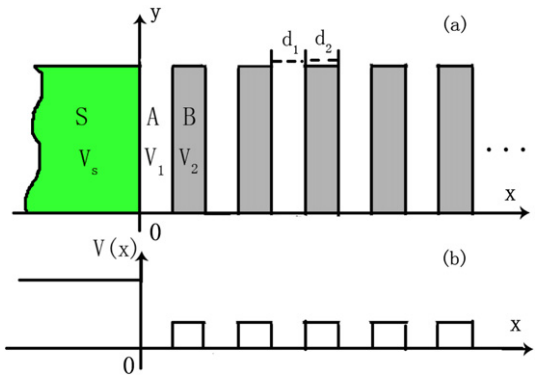

Fig. 1. (a) Schematic of the graphene-based heterostructure. Non-white regions denote the graphene with electrostatic potentials. $d_1 = d_2 = 30$ nm. The interface between the homogeneous graphene S and (AB) superlattice is at $x = 0$. (b) The profiles of the potential applied on the monolayer graphene.

Firstly, we deduce the dispersion equation of (AB) superlattice. In the jth potential, the wave function of ψ_A has the common form [37]:

$$\psi_A(x) = a_j e^{iq_j(x-x_j)} + b_j e^{-iq_j(x-x_j)} \quad (x_{j-1} < x < x_j), \tag{4}$$

where $q_j = \sqrt{k_j^2 - \beta^2}$ is the x component of the wave vector in the jth potential, a and b are the coefficients of the forward and backward spinor components, respectively, x_j is the position of the interface of the jth and the $(j+1)$th potentials. Substituting Eq. (4) into Eq. (2), in the jth potential we obtain

$$\psi_B(x) = a_j\frac{ik_j}{iq_j+\beta}e^{iq_j(x-x_j)} - b_j\frac{ik_j}{iq_j-\beta}e^{-iq_j(x-x_j)}. \tag{5}$$

Assuming that $\eta_j = \frac{ik_j}{iq_j+\beta}$, $\gamma_j = \frac{ik_j}{iq_j-\beta}$, ψ_B can be rewritten as

$$\psi_B(x) = a_j\eta_j e^{iq_j(x-x_j)} - b_j\gamma_j e^{-iq_j(x-x_j)}. \tag{6}$$

From Eqs. (4) and (6), we have

$$\begin{pmatrix}\psi_A\\ \psi_B\end{pmatrix} = D_j\begin{pmatrix}a_j e^{iq_j(x-x_j)}\\ b_j e^{-iq_j(x-x_j)}\end{pmatrix}, \tag{7}$$

where $D_j = \begin{pmatrix}1 & 1\\ \eta_j & -\gamma_j\end{pmatrix}$.

When the wave function runs across the interface of the jth and $(j+1)$th potentials, the boundary conditions require that $\psi_A(x_j^-) = \psi_A(x_j^+)$ and $\psi_B(x_j^-) = \psi_B(x_j^+)$. This means

$$D_j\begin{pmatrix}a_j\\ b_j\end{pmatrix} = D_{j+1}\begin{pmatrix}a_{j+1}\\ b_{j+1}\end{pmatrix}, \tag{8}$$

where $D_{j+1} = \begin{pmatrix}1 & 1\\ \eta_{j+1} & -\gamma_{j+1}\end{pmatrix}$.

Eq. (8) can be rewritten as

$$\begin{pmatrix}a_{j+1}\\ b_{j+1}\end{pmatrix} = D_{j+1}^{-1}D_j\begin{pmatrix}a_j\\ b_j\end{pmatrix}, \tag{9}$$

where the inverse matrix $D_{j+1}^{-1} = \frac{1}{\eta_{j+1}+\gamma_{j+1}}\begin{pmatrix}\gamma_{j+1} & 1\\ \eta_{j+1} & -1\end{pmatrix}$.

Assuming $D_{(j+1)j} = D_{j+1}^{-1}D_j$, this matrix connects the forward and backward coefficients from one side of the interface to the other side. Considering the wave transport inside the jth potential, one can obtain the matrix connecting the forward and backward wave coefficients in one potential with those in the other potential separated by a unit cell as follows:

$$\begin{pmatrix}a_n\\ b_n\end{pmatrix} = M\begin{pmatrix}a_{n+1}\\ b_{n+1}\end{pmatrix}, \tag{10}$$

where $M = P_j D_{j(j+1)} P_{j+1} D_{(j+1)j}$ in which $P_j = \begin{pmatrix} e^{-iq_j d_j} & 0 \\ 0 & e^{iq_j d_j} \end{pmatrix}$, and n denotes the nth period. On the other hand, according to the Bloch–Floquet theorem, we have

$$\begin{pmatrix} a_n \\ b_n \end{pmatrix} = e^{iKd} \begin{pmatrix} a_{n+1} \\ b_{n+1} \end{pmatrix}, \tag{11}$$

where K is Bloch wave vector, and $d = d_1 + d_2$ is the length of the unit cell. From Eqs. (10) and (11), we obtain the eigen-equation as follows:

$$\left(M - e^{iKd}\hat{I}\right) \begin{pmatrix} a_n \\ b_n \end{pmatrix} = 0. \tag{12}$$

Assuming $M = \begin{pmatrix} A & B \\ C & D \end{pmatrix}$, from Eq. (12) we can obtain the following dispersion equation for band diagram,

$$e^{iKd} = \frac{1}{2}\left[(A+D) \pm \sqrt{(A+D)^2 - 4}\right], \tag{13}$$

in which band edges correspond to $|\frac{1}{2}(A+D)| = 1$.

When $n = 0$, $e^{iKd}\begin{pmatrix} a_0 \\ b_0 \end{pmatrix} = M\begin{pmatrix} a_0 \\ b_0 \end{pmatrix}$ and thereafter we obtain

$$\begin{pmatrix} a_0 \\ b_0 \end{pmatrix} = \begin{pmatrix} B \\ e^{iKd} - A \end{pmatrix}. \tag{14}$$

So, the wave functions at the entrance face of superlattice can be derived by $\begin{pmatrix} \psi_{A0} \\ \psi_{B0} \end{pmatrix} = D_0 \begin{pmatrix} a_0 \\ b_0 \end{pmatrix}$.

Now we deduce the dispersion equation of Tamm states in the heterostructures. As shown in Fig. 1, the interface between the homogeneous graphene S and (AB) superlattice is at $x = 0$. For waves localized at the interface, the wave functions on the left side of the interface can be expressed as:

$$\begin{cases} \psi_{As} = a_s e^{q_s x} \\ \psi_{Bs} = a_s \gamma_s e^{q_s x} \end{cases} \quad (x < 0, q_s > 0), \tag{15}$$

where $\gamma_s = \frac{ik}{q_s + \beta}$. While on the right side of the interface, i.e., inside the superlattice, the wave functions are decaying Bloch waves. The boundary conditions at $x = 0$ require that

$$\begin{pmatrix} \psi_{A0} \\ \psi_{B0} \end{pmatrix} = \begin{pmatrix} \psi_{As} \\ \psi_{Bs} \end{pmatrix}. \tag{16}$$

Substituting Eqs. (14) and (15) into Eq. (16), we finally obtain the dispersion equation of Tamm states as follows:

$$\frac{ik}{q_s + \beta} = \frac{B\eta_0 - (e^{iKd} - A)\gamma_0}{B - A + e^{iKd}}. \tag{17}$$

3. Dispersion diagram and amplitude distributions

Here we numerically solve the dispersive equation (17). The value of the left (right) side of Eq. (17) is denoted by Val_L (Val_R). In the following calculations, we assume $d_1 = d_2 = 30$ nm. Firstly, we suppose $V_1 = 0$ meV, $V_2 = 20$ meV, $V_s = 54$ meV and fix the value of β, e.g., $\beta = 0.45k_0$, where $k_0 = 45(\mathrm{meV})/\hbar\upsilon_F$, and we solve the electronic energy satisfying Eq. (17). In Fig. 2, we draw the real and imaginary parts of Val_L [in solid lines with open (solid) circles] and Val_R [in solid lines with open (solid) squares] as a function of energy, respectively. One can see in the forbidden gap corresponding to energies above 44.5 meV, the real parts of both Val_L and Val_R go to zero. Also, within the forbidden gap, there is a cross point of the imaginary parts of Val_L and Val_R. The abscissa value at the cross point (44.9 meV) is the energy solution of Eq. (17) at $\beta = 0.45k_0$. Based on the above method, we vary the value of β and derive each corresponding value of energy. Then we draw the dispersive curve of Tamm states, as shown by the solid line in Fig. 3. The allowed bands (in shaded regions) and forbidden gaps (in white regions) of the AB superlattice are also shown in Fig. 3 by solving Eq. (13). The value of β is normalized by $k_0 = 45(\mathrm{meV})/\hbar\upsilon_F$. It should be pointed out that the spectrum is symmetric with respect to the change of sign of β. In Fig. 3, one can that see no Tamm state occurs in the first gap. In the second gap, at small β (see the inset in Fig. 3) the slope of the dispersive curve is negative and at larger β it remains positive. Since the slope of the dispersive curve corresponds to the group velocity of the Tamm states, for small β the Tamm states are backward states in which the signs of E/β and $\partial E/\partial\beta$ are opposite. Moreover, if we vary the value of V_s, the magnitude as well as the sign of the slope of the dispersive curve of Tamm states can be tuned, as shown by the dashed line when $V_s = 62$ meV and the dot-dashed line when $V_s = 70$ meV in Fig. 3. It is also seen that each Tamm dispersive curve corresponding to a value of V_s has a cutoff β at the minimum energy. Besides, the larger the value of V_s is, the larger the cutoff value of β is and the deeper the Tamm states are inside the gap. This can be qualitatively explained as follows. For a Tamm state, the value of wave vector vertical to the interface inside the homogeneous graphene, i.e., $k_{sx} = \sqrt{k_s^2 - \beta^2} = \sqrt{[(E - V_s)/\hbar\upsilon_F]^2 - \beta^2}$, should be complex. When the energy E is within the gap, for a given value of V_s, β should have a nonzero cutoff value to make k_{sx} a complex number. While between zero and the cutoff value of β, the electronic states with propagating wave vectors inside the homogeneous graphene become extended states. Moreover, in $E < V_s$ case, the larger the value of V_s is, the larger the cutoff value of β is. On the other hand, with the increase of β, the width of the gap is broadened. The enlarged gap strengthens the confinement to the Tamm states and makes them deeper inside the gap. It is known that a weak localized electronic state is apt to broadening, e.g., due to electron–phonon interaction. However, a strong localized Tamm state that is deep inside the gap is robust against the external disturbance.

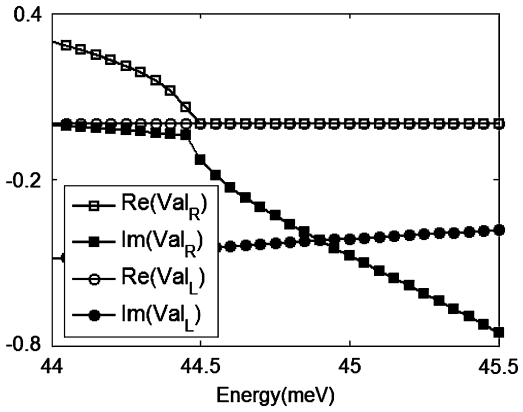

Fig. 2. Real and imaginary parts of the values of left side denoted by Val_L (in solid lines with circles) and right side denoted by Val_R (in solid lines with squares) of Eq. (17) versus energy, respectively. $V_1 = 0$ meV, $V_2 = 20$ meV, $V_s = 54$ meV, and $\beta = 0.45k_0$, where $k_0 = 45(\mathrm{meV})/\hbar\upsilon_F$. In the forbidden gap (energy higher than 44.5 meV), $\mathrm{Re}(\mathrm{Val}_L) = \mathrm{Re}(\mathrm{Val}_R) \equiv 0$, and the abscissa value (44.9 meV) at the cross point of $\mathrm{Im}(\mathrm{Val}_L)$ and $\mathrm{Im}(\mathrm{Val}_R)$ is the energy solution of Eq. (17).

To know the physical origin of the backward Tamm states, in Figs. 4(a) and 4(b) we calculate the profiles of probability amplitudes corresponding to the points (a) and (b) in Fig. 3, respectively. For points (a) and (b), the values of β are 0.203 and 0.283, respectively, and the values of energy are both 44.9 meV. Blue solid lines and red dashed lines denote the probability amplitudes of ψ_A and ψ_B, respectively. In left-handed homogeneous graphene the directions of wave vector and group velocity are opposite while in AB superlattice their directions are the same. Besides, the directions of parallel wave vectors in homogeneous graphene and superlattice should be same, as required by the

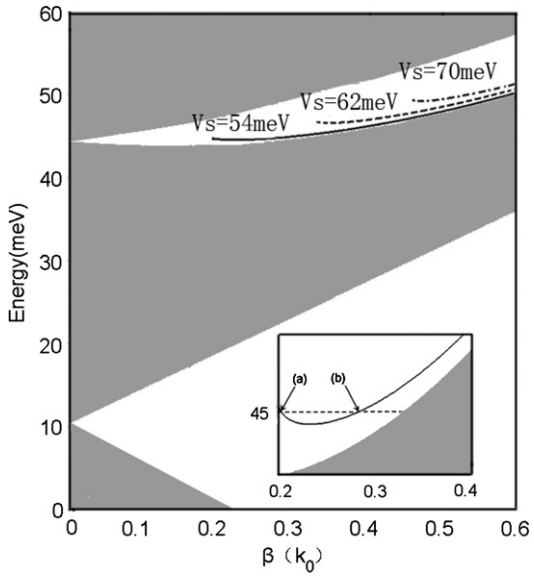

Fig. 3. Dispersion diagram of the Tamm states in electronic gaps. The solid line: $V_s = 54$ meV; the dashed line: $V_s = 62$ meV; the dot-dashed line: $V_s = 70$ meV. The shaded and white regions denote the allowed bands and forbidden gaps of (AB) superlattice, respectively. The value of β is normalized by $k_0 = 45(\text{meV})/\hbar\upsilon_F$. Inset shows a blowup region of the solid line at smallβ. Points (a) and (b) in the inset correspond to the profiles of probability amplitudes shown in Figs. 4(a) and 4(b), respectively.

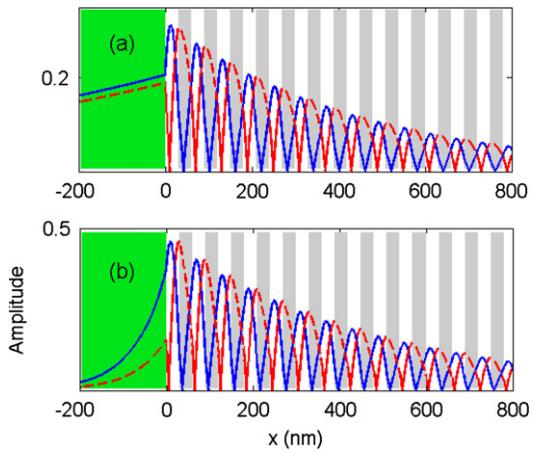

Fig. 4. Examples of the electronic Tamm states at 44.9 meV. (a) Backward electronic state corresponding to the point (a) in Fig. 3. $\beta = 0.203$. (b) Forward state corresponding to the point (b) in Fig. 3. $\beta = 0.283$. Blue solid lines and red dashed lines denote the probability amplitudes of ψ_A and ψ_B, respectively. (For interpretation of the references to colour in this figure legend, the reader is referred to the web version of this Letter.)

boundary conditions. Therefore, whether the group velocity of the Tamm states is parallel or antiparallel with wave vector depends on the decaying rate of amplitudes of waves into homogeneous graphene and superlattice [40]. In Fig. 4(a), one can see that the amplitudes of waves decay more rapidly from the surface into superlattice (see the wave envelop) than into homogeneous graphene. So on the whole, the group velocity of the Tamm states is antiparallel with wave vector, which corresponds to the backward Tamm states. In contrast, in Fig. 4(b) the amplitudes of waves decay more rapidly from the surface into homogeneous graphene than into superlattice, leading to the forward Tamm states.

For comparison, we also show a case that Tamm states occur when the homogeneous graphene is not left-handed (in the

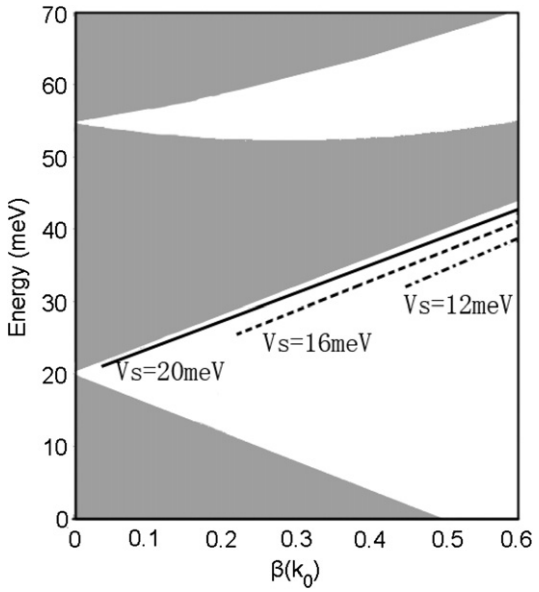

Fig. 5. Dispersion diagram of Tamm states occurring in the $E > V_s$ region. $V_1 = 0$ meV and $V_2 = 40$ meV. The solid line: $V_s = 20$ meV; the dashed line: $V_s = 16$ meV; the dot-dashed line: $V_s = 12$ meV.

$E > V_s$ region). Setting $V_1 = 0$ meV and $V_2 = 40$ meV, we choose three different values of V_s (20 meV, 16 meV, 12 meV) and calculate the corresponding Tamm dispersive curves, as shown by the solid line, the dashed line and the dot-dashed line, respectively, in Fig. 5. In contrast to Fig. 3, in Fig. 5 one can see that no Tamm state occurs in the second gap. In the first gap, all the Tamm dispersive curves have positive slope. This means all the Tamm states are forward states that are similar to those in a truncated crystal or a conventional superlattice. Moreover, in the $E > V_s$ case, the smaller the value of V_s is, the larger the cutoff value of β is and the deeper the Tamm states are inside the gap. On the whole, the graphene-based heterostructure greatly extends our control over the group velocity of Tamm states since we can realize either forward or backward Tamm states just by changing the applied voltage.

4. Conclusions

In conclusion, Tamm states in graphene-based heterostructures applied by suitable electrodes are theoretically studied. The adjustable external voltage provides us more freedom to tune the dispersive properties of Tamm state and especially can support the backward Tamm state in which the direction of the wave vector of the electronic surface wave reverses with that of the group velocity. If we can predict or even tune the surface states as well as their effects on the potential, carrier transport, etc., of a material, then we can gain a better understanding of how to operate a device of this material. So the tunable Tamm states, together with the peculiar properties of Dirac electrons, would be very useful in potential device applications.

Acknowledgements

This research was funded by the National Basic Research Program of China (grant No. 2011CB922001), by the National Natural Science Foundation of China (grant Nos. 11074187 and 51007064), and by the Program for Key Basic Research of the Shanghai Science and Technology Committee (grant No. 08dj1400301).

References

[1] K.S. Novoselov, A.K. Geim, S.V. Morozov, D. Jiang, Y. Zhang, S.V. Dubonos, I.V. Grigorieva, A.A. Firsov, Science 306 (2004) 666.
[2] K.S. Novoselov, A.K. Geim, S.V. Morozov, D. Jiang, M.I. Katsnelson, I.V. Grigorieva, S.V. Dubonos, A.A. Firsov, Nature (London) 438 (2005) 197.
[3] C.W.J. Beenakker, Rev. Mod. Phys. 80 (2008) 1337;
A.H. Castro Neto, F. Guinea, N.M.R. Peres, K.S. Novoselov, A.K. Geim, Rev. Mod. Phys. 81 (2009) 109.
[4] M.I. Katsnelson, K.S. Novoselov, A.K. Geim, Nat. Phys. 2 (2006) 620;
A.F. Young, P. Kim, Nat. Phys. 5 (2009) 222.
[5] Y. Zhang, Y.W. Tan, H.L. Stormer, P. Kim, Nature (London) 438 (2005) 201;
K.I. Bolotin, F. Ghahari, M.D. Shulman, H.L. Stormer, P. Kim, Nature (London) 462 (2009) 196.
[6] F. Wang, Y. Zhang, C. Tian, C. Girit, A. Zettl, M. Crommie, Y.R. Shen, Science 320 (2008) 206.
[7] V.S. Veselago, Sov. Phys. Usp. 10 (1968) 509.
[8] V.V. Cheianov, V. Fal'ko, B.L. Altshuler, Science 315 (2007) 1252.
[9] V.M. Agranovich, Yu.N. Gartstein, Phys. Usp. 49 (2006) 1029.
[10] J.L. Garcia-Pomar, A. Cortijo, M. Nieto-Vesperinas, Phys. Rev. Lett. 100 (2008) 236801.
[11] A.G. Moghaddam, M. Zareyan, Phys. Rev. Lett. 105 (2010) 146803.
[12] C. Bai, X. Zhang, Phys. Rev. B 76 (2007) 075430.
[13] C.-H. Park, L. Yang, Y.-W. Son, M.L. Cohen, S.G. Louie, Nat. Phys. 4 (2008) 213.
[14] M. Barbier, F.M. Peeters, P. Vasilopoulos, J.M. Pereira, Phys. Rev. B 77 (2008) 115446.
[15] C.-H. Park, L. Yang, Y.-W. Son, M.L. Cohen, S.G. Louie, Phys. Rev. Lett. 101 (2008) 126804.
[16] M. Barbier, P. Vasilopoulos, F.M. Peeters, Phys. Rev. B 81 (2010) 075438.
[17] M. Ramezani Masir, P. Vasilopoulos, A. Matulis, F.M. Peeters, Phys. Rev. B 77 (2008) 235443.
[18] L. Dell'Anna, A. De Martino, Phys. Rev. B 79 (2009) 045420;
L. Dell'Anna, A. De Martino, Phys. Rev. B 80 (2009) 155416.
[19] F. Guinea, M.I. Katsnelson, M.A.H. Vozmediano, Phys. Rev. B 77 (2008) 075422;
A. Isacsson, L.M. Jonsson, J.M. Kinaret, M. Jonson, Phys. Rev. B 77 (2008) 035423.
[20] J.C. Meyer, C.O. Girit, M.F. Crommie, A. Zettl, Appl. Phys. Lett. 92 (2008) 123110.
[21] A.L. Vázquez de Parga, F. Calleja, B. Borca, M.C.G. Passeggi Jr., J.J. Hinarejos, F. Guinea, R. Miranda, Phys. Rev. Lett. 100 (2008) 056807.
[22] I. Pletikosić, M. Kralj, P. Pervan, R. Brako, J. Coraux, A.T. N'Diaye, C. Busse, T. Michely, Phys. Rev. Lett. 102 (2009) 056808.
[23] K.S. Kim, Y. Zhao, H. Jang, S.Y. Lee, J.M. Kim, K.S. Kim, J.-H. Ahn, P. Kim, J.-Y. Choi, B.H. Hong, Nature (London) 457 (2009) 706.
[24] R. Tsu, Superlattice to Nanoelectronics, Elsevier, Oxford, 2005.
[25] L. Brey, H.A. Fertig, Phys. Rev. Lett. 103 (2009) 046809.
[26] C.H. Park, Y.W. Son, L. Yang, M.L. Cohen, S.G. Louie, Phys. Rev. Lett. 103 (2009) 046808.
[27] R.P. Tiwari, D. Stroud, Phys. Rev. B 79 (2009) 205435.
[28] M. Barbier, P. Vasilopoulos, F.M. Peeters, Phys. Rev. B 80 (2009) 205415.
[29] C.-H. Park, Y.-W. Son, L. Yang, M.L. Cohen, S.G. Louie, Nano Lett. 8 (2008) 2920.
[30] L.G. Wang, S.Y. Zhu, Phys. Rev. B 81 (2010) 205444.
[31] F.D.M. Haldane, S. Raghu, Phys. Rev. Lett. 100 (2008) 013904.
[32] Z. Wang, Y.D. Chong, J.D. Joannopoulos, M. Soljacic, Nature (London) 461 (2009) 772.
[33] X. Zhang, Phys. Lett. A 372 (2008) 3512;
S.R. Zandbergen, Michiel J.A. de Dood, Phys. Rev. Lett. 104 (2010) 043903.
[34] I. Tamm, Phys. Z. Sowjetunion 1 (1932) 733.
[35] H. Ohno, E.E. Mendez, J.A. Brum, J.M. Hong, F. Agulló-Rueda, L.L. Chang, L. Esaki, Phys. Rev. Lett. 64 (1990) 2555.
[36] P. Yeh, A. Yariv, A.Y. Cho, Appl. Phys. Lett. 32 (1978) 104.
[37] P. Yeh, Optical Waves in Layered Media, Wiley, New York, 1988.
[38] J. Martorell, D.W.L. Sprung, G.V. Morozov, J. Opt. A, Pure Appl. Opt. 8 (2006) 630.
[39] N. Malkova, C.Z. Ning, Phys. Rev. B 73 (2006) 113113.
[40] A. Namdar, I.V. Shadrivov, Y.S. Kivshar, Appl. Phys. Lett. 89 (2006) 114104;
A. Namdar, I.V. Shadrivov, Y.S. Kivshar, Phys. Rev. A 75 (2007) 053812.